Deformation in the Rutford ice stream, West Antarctica: measuring shear-wave anisotropy using icequakes.

S.R. Harland[a], J-M. Kendall[b], G. W. Stuart[a], G. E. Lloyd[a], A. F. Baird[b], A. M. Smith[c], H. D. Pritchard[c], A. M. Brisbourne[d]

[a]*School of Earth and Environment, The University of Leeds, Leeds, LS2 9JT, UK.*

[b]*Department of Earth Sciences, University of Bristol, Wills Memorial Building, Bristol, BS8 1RJ, UK.*

[c]*British Antarctic Survey, Madingley Road, High Cross, Cambridge, Cambridgeshire, CB3 0ET, UK.*

[d]*SEIS-UK, Geology Department, University of Leicester, University Road, Leicester, LE1 7RH, UK.*

Abstract

Ice streams provide major drainage pathways for the Antarctic ice sheet. The stress distribution and style of flow in such ice streams produces elastic and rheological anisotropy, which informs ice flow modelling as to how ice masses respond to external changes such as global warming. Here we analyse elastic anisotropy in the Rutford ice stream, West Antarctica, using observations of shear wave splitting from three-component icequake seismograms to characterise ice deformation via crystal preferred orientation. Over 110 high quality measurements are made on 41 events recorded at five stations temporarily deployed near the ice stream grounding line. To the best of our knowledge this is the first well-documented observation of shear wave splitting from Antarctic icequakes. The magnitude of the splitting ranges from 2ms to 80ms and suggest a maximum of 6% shear wave splitting. The fast shear wave polarisation direction is roughly perpendicular to ice flow direction. We consider three mechanisms for ice anisotropy: a cluster model (VTI model); a girdle model (and HTI model); and crack-induced anisotropy (an HTI model). Based on the data we can rule out a VTI mechanism as the sole cause of anisotropy – an HTI component is needed, which may be due to ice crystal a-axis alignment in the direction of flow or the alignment of cracks or ice-films in the plane perpendicular to the flow direction. The results may suggest a combination of

mechanisms are at play, which represent vertical variations in the symmetry of ice-crystal anisotropy in an ice stream, as predicted by ice fabric models.

Introduction

Ice streams account for only 10% of the Antarctic ice sheet, but are areas of significantly enhanced flow that are responsible for nearly 90% of the ice sheet drainage (Morgan et al., 1982). Tracking the internal movement and deformation of ice streams is key to understanding how they operate and respond to external factors. The deformation history of ice is preserved as elastic anisotropy due to the crystal preferred orientation (CPO) of ice crystals (eg., Alley, 1988). Therefore in-situ detection of such anisotropy is desirable, as it offers insights into stress patterns and the behaviour of ice sheets over time and over large areas. It also provides a means of testing the influence of crystal fabric on patterns of ice sheet flow (Martin et al, 2009), information that is needed to calibrate ice sheet modelling. Deformation along the margins of ice-streams leads to crevassing and fracturing, and basal reflectors of radar and seismic signals have been attributed oriented crystal (CPO) fabrics (e.g., King, 2009; Horgan et al., 2011). Here we investigate ice anisotropy in the Rutford ice-stream, West Antarctica, using observations of shear-wave anisotropy in recordings of icequakes.

The Rutford ice-stream is a major ice-stream in West Antarctica that drains into the Ronne Ice Shelf. Situated in a deep trough between the Ellsworth Mountains and the Fletcher Promontory, this roughly 300 km long, 25 km wide and 2.5 km thick ice-stream moves at speeds up to 400 meters per year. During the Austral summer of 2008-09, a team from the British Antarctic Survey (BAS) deployed an array of three-component seismometers on the Rutford ice stream (Pritchard et al, 2011, Brisbourne, 2012). Many thousands of microseismic events (icequakes) were recorded during the experiment, which only lasted a few weeks. The slippage of ice over the underlying rock bed leads to icequakes, especially in spots where there is little fluid-saturated basal sediment to lubricate the sliding (Anandakrishnan and Bentley, 1993; Anandakrishnan and Alley, 1994; Walter et al., 2008). An attractive feature of icequakes is that they generate P-waves and S-waves, and many conventional tools from earthquake

seismology can be applied to such data. We analyse shear-wave anisotropy using a high-quality subset of this dataset.

Elastic anisotropy is found in most parts of the solid Earth and can be caused by a range of mechanisms (Backus, 1962; Blackman et al., 2002; Holtzman and Kendall, 2010). We consider candidate crystal fabrics due to CPO found in ice as plausible mechanisms for anisotropy in an ice stream environment. We also consider a more extrinsic mechanism where anisotropy can be caused by preferentially aligned cracks or melt films; the possibility of such oriented weaknesses will have ramifications for the disintegration of ice shelves fed by ice streams.

Mechanisms for anisotropy in ice.

Anisotropy refers to a directional variation in wave speeds and leads to a more complicated description of wave propagation than that for isotropic media. Only two elastic parameters are required to describe wave propagation in an isotropic medium, whereas up to 21 independent elastic constants are required to describe waves propagation in anisotropic media. The perhaps most tell-tale sign of anisotropy is the presence of two independently propagating shear-waves (so-called shear-wave splitting). An initially polarised shear-wave travelling through an isotropic medium, will split into two orthogonally polarised shear waves as it impinges on a region of anisotropy. The polarisation of the shear-waves is diagnostic of the anisotropic symmetry and the delay time between the fast and slow shear waves is a proxy for the magnitude of the anisotropy and the extent of the anisotropic region.

It is well known that ice crystals are anisotropic and that they can exhibit a CPO fabric (e.g., Alley, 1988; Budd and Jacka, 1989; Wilson and Zhang, 1994). Hexagonal ice (Ih), the form naturally found on Earth, has two principal crystal axes: a vertical c-axis and three a-axes separated by 120^{o} and normal to the c-axis. The c-axis provides a major axis of symmetry in the elastic properties of the crystal and velocities are rotationally invariant around this axis (often termed transverse isotropy). The direction of fastest P-wave velocity is along the c-axis (3.89 km/s) and the slowest velocities are found in a roughly 50^{o} cone from the c-axis (3.74 km/s). The direction of minimum (0 km/s) shear-wave splitting is

along the c-axis and the direction of maximum (0.24 km/s) shear-wave splitting (i.e., separation between the fast and slow shear wave) is roughly 50° from the c-axis (Figure 1a) The slowest shear wave velocity is along the c-axis (1.81 km/s), whilst the fastest (2.10 km/s) midway between the c- and a-axes.

Ice crystals shear two orders of magnitude more easily along the basal plane (orthogonal to the c-axis) than on the other slip systems (Duval et al., 1983), which readily leads to a CPO primarily by dislocation glide (e.g., Castelnau, 1996). As ice sheets flow and deform, the constituent crystals will align depending on factors such as strain rates, temperature and the presence of fluids. The resulting CPO can be very effective in producing an anisotropic medium.

In the near-surface, ice has a random fabric of crystals where the c- and a-axes are distributed through all possible orientations. When stress is applied, 90% of the deformation is accommodated by slip on the basal plane parallel to an a-axis direction, restricted by neighbouring grains (Wilson, 2000). Flattening under gravity or weight causes ice crystals to rotate such that the c-axes rotate towards the compressive stress (i.e., vertical) and the a-axes rotate uniformly away from the compression into the perpendicular plane (Alley, 1988). With depth and increasing hydrostatic pressure, the c-axes orient themselves into a cone about the vertical axis, forming a cluster fabric (Wilson, 2000) and producing a transversely isotropic medium with a vertical symmetry axes (a so-called VTI, vertical transversely isotropic, symmetry) (Figure 1b). The angle this cone makes to the vertical decreases with increasing hydrostatic pressure. In structural geology, such a CPO is known as a cluster fabric, whereas in glaciology this CPO is normally referred to as the solid cone fabric (e.g. Horgan et al, 2011). Compared to the single crystal anisotropy, the P-wave and S-wave anisotropy is less, but the overall symmetry of the anisotropy is similar. At even greater depths the effects of dynamic recrystallisation may lead to a more random orientation in the c-axes and hence a weaker overall anisotropy (Anandakrishnan et al., 1994).

In an ice stream, the ice can be also confined perpendicular to the flow (stress) direction, resulting in simple shear (Azuma, 1994). As such, the a-axes develop a preferred orientation parallel to the flow and the c-axes rotate into a girdle distribution orthogonal to the flow direction (Alley, 1988; Wilson, 2000)

(Figure 1c). This effectively produces a transversely isotropic medium with a horizontal symmetry axis, which is often referred to as HTI (horizontal transversely isotropic) symmetry. In this model the fastest P-wave (3.88 km/s) is orientated in the ice-flow or a-axis direction. The vertical plane parallel to the flow direction is the plane of maximum shear-wave splitting (0.08 km/s).

Azuma (1994) derived a flow law for anisotropic ice and developed a model of ice fabric distributions within a flowing ice stream (Figure 2) based on the flow law predictions for three different flow regimes: divergent flow from the theoretical point source of an ice stream/glacier; parallel flow in the laterally constricted area of an ice stream/glacier; and convergent flow to the theoretical point outlet of an ice stream/glacier. As can be seen from (Figure 2) the lower 1/3 of the ice stream is dominated by the shear zone and cluster fabric, independent of flow regime. However the upper 2/3 of each regime has variable fabric depending on the flow regime. SEM (scanning electron microscopy) and EBSD (electron back-scatter diffraction) analysis of Vostok ice core by Obbard and Baker (2007) demonstrated that the depth dependent CPO fabrics modelled by Azuma (1994) do exist within the Antarctic ice. The majority of the core is dominated by a girdle fabric. Only at shallow depths is the orientation random and only towards the very base of the ice do cluster fabrics begin to appear.

Another mechanism that is very effective in producing anisotropy is the alignment of cracks or melt films (Kendall et al., 2007), which is sometime referred to as a shape-preferred orientation (SPO). A material with an aligned set of cracks will behave as an effectively homogeneous, but anisotropic medium, as long as the seismic wavelength is much larger than the crack spacing. Aligned vertical cracks can be treated as an HTI medium. Depending on the wetting angle, melt-films in glaciers can be ellipsoidal in shape (Mader et al., 1992), and if aligned, will be very effective in producing anisotropy. Alternatively, the alignment of larger cracks and fissures will also be effective in generating a seismic anisotropy. Distinguishing between a more intrinsic anisotropy due to ice-crystal alignment and a more extrinsic mechanisms due to crack alignment can be challenging and requires datasets with very good angular coverage in raypaths (Verdon et al., 2009).

In-situ measurements of ice anisotropy.

There are many seismic methods for studying elastic anisotropy using both body waves and surface waves (e.g., Brisbourne et al., 1999; Kendall et al., 2007). A potential problem with P-wave studies is the trade-off between heterogeneity along the ray paths and anisotropy. Icequakes are very efficient in generating shear-waves, and with accurate source locations one can study shear-wave anisotropy along the raypath. Measurements from multiple raypaths can be then used to constrain the style of anisotropy (e.g., Verdon et al., 2009).

In a series of remarkable Antarctic seismic experiments in the late 1960s and early 1970s our knowledge of ice anisotropy advanced significantly (see summary in Bentley, 1975). Acharya (1972) used surface wave dispersion measurements to estimate 8-10% shear-wave anisotropy in the ice cap at Byrd Land. He attributed this to near-surface layering in the upper few 100m of ice (see Backus (1962) for a description of the mechanism). Robinson (1968) considered body and surface wave data across the polar plateau and the Ross Ice Shelf, showing that the near-surface velocity of the plateau was isotropic, whilst the Ross Ice Shelf exhibited nearly 20% P-wave anisotropy. In a series of experiments, Bentley (1971) observed azimuthal variations of P-waves from refraction and wide-angle reflection data, which he related to the CPO of ice crystals. He also observed shear-wave splitting in converted P-S reflections. In an earlier refraction experiment, Bentley (1964) observed nearly 30 ms of shear-wave splitting (birefringence) between vertically (Sv) and horizontally (Sh) polarised shear waves that propagated for over 6.5 seconds.

The connection between ice fabric and seismic velocities was better established using ultrasonic measurements in a deep borehole at Byrd Station (Bentley, 1972). This work showed P-wave anisotropy at depths greater than 400m, which increased dramatically at depths greater than 1200m, but then decreased again below 1800m. A notable conclusion from this work is the depth-dependent variations in the symmetry of the ice anisotropy, where near vertical c-axes orientation was inferred in the deeper parts of the ice sheets, but a double cluster or asymmetry in c-axes clustering was observed at intermediate depths. Anandakrishnan et al. (1994) used both compressional and shear-wave transducers to study c-axes alignment in ice core from Greenland. They showed a

199 decrease with depth in the solid-cone angle the c-axes make to the vertical, but
200 also noted some asymmetry in the clustering. Most recently Gusmeroli et al.
201 (2012) have established a theoretical basis for using borehole sonic logging to
202 assess the fabric of polycrystalline glacial ice. Cumulatively, these studies have
203 shown that ice anisotropy may vary both laterally and with depth in ice masses.
204
205 **The icequake dataset**
206 The microseismic dataset was collected in the Austral summer of 2008-
207 09 (between December 2008 and February 2009). Ten stations of high frequency
208 (1kHz), 3-component geophones were deployed in two arrays of five stations
209 (Pritchard et al., 2011). The horizontal components were orientated parallel
210 (North Component) and perpendicular (East Component) to the ice flow
211 direction. Each instrument was buried at a depth of 1m to reduce ambient noise
212 and increase coupling by lying below fresh snow.
213 Array locations were guided by the results of previous reflection and
214 micro-seismic surveys (Smith 1997a; Smith, 1997b; Smith, 2006). The South
215 array was sited over an area of harder bed, where basal sliding occurs, whereas
216 the North array was sited above an area of deformable sediment (Smith, 2006).
217 Data from the South array were used in this study as it recorded many more
218 events, owing to the array being over a high friction 'sticky spot' (Smith, 2006).
219 Here we analyse 250 events recorded by all 5 stations over the course of a single
220 day.
221 Only events with high signal-to-noise ratios (SNR) are analysed and
222 acceptable events had clear P-wave arrivals on at least 4 stations. In many cases,
223 the fast and slow shear waves were clearly visible on the unrotated
224 seismograms, presumably due to the orientation of the horizontal components
225 with the flow direction. Figure 3 shows an example of a typical high SNR event.
226 The events were located using a non-linear inversion of P- and S-wave
227 travel times (HYPO2000, Klein, 2000). Due to a lack of knowledge of the velocity
228 structure of the Rutford ice sheet, a homogeneous isotropic model was assumed.
229 Based on Roethlisberger (1972), the P-wave velocity (Vp) was assumed to be
230 3.60 km/s and S-wave velocity (Vs) 1.85 km/s, giving a Vp/Vs ratio of 1.95. The
231 travel time of the earliest arriving S-wave signal was used in the inversion. Not

all events could be located due to intermittent failure of one of the stations. The total number of successfully located events was 41 (Figure 4), most of which were located close to the base of the ice, estimated from radar imaging (King, 2009).

Clusters of events are revealed by similar S-P travel times and waveforms, showing that events occur repeatedly at the same locations throughout the day (Figure 4). The error in estimated depth of the events is much larger than lateral location errors (100s meters versus 10s meters). Location errors are most likely due to a lack of detailed knowledge of the velocity structure of the ice stream. Preliminary analysis of focal mechanisms derived from first-motions, suggest low-angle thrust mechanisms, consistent with stick-slip stress release at the base of the ice stream.

Shear-wave splitting analysis

For a given event, shear-wave splitting is measured for each station using the approach of Wuestefeld et al. (2010). The analysis estimates the splitting parameters ϕ (which is the polarisation of the fast shear-wave) and δt (the time delay between the fast and slow shear-waves). A grid search over all possible fast shear-wave polarisations and delay times (up to 100 ms) is used to find the splitting parameters that best linearise the particle motion, thus removing the effects of the anisotropy. In practice the grid search minimises the second eigenvalue of the covariance matrix of the S-wave signal recorded on the two horizontal components. The analysis is done on 100 windows around the S-wave and a cluster analysis is used to assess the stability of the solution (Teanby et al., 2004). A statistical f-test is used to assess the errors in the estimates of the splitting parameters. The analysis also estimates the initial S-wave polarisation at the source. So-called 'null' results occur when the medium is isotropic or when the initial source polarisation is aligned with the fast or slow shear-wave polarisation. Inconclusive results and high error estimates occur when the data are noisy.

Figure 5 shows an example of a shear-wave splitting measurement on an icequake. The clear separation between the fast and slow shear-wave is apparent on the unrotated data (Figure 3), which leads to an x-shaped S-wave particle

motion. Such an observation is very unusual in conventional earthquakes data. A more familiar elliptical particle motion is observed when the delay time (δt) is less than the dominant period of the S-waves (see, e.g., Wuestefeld et al., 2010). The splitting analysis linearises the particle motion and minimises the S-wave energy on the component aligned perpendicular to the initial S-wave polarisation.

With surface sensors, the splitting analysis can be only performed when the raypath direction is less than the 45 degrees to the vertical (i.e., within the shear-wave window). At greater angles, free-surface effects can generate elliptical particle motion in the S-wave arrivals (Booth and Crampin, 1985).

The analysis produces 111 reliable shear wave splitting measurements from the 41 events that were considered. Events with errors in ϕ greater than 10^{o} were discarded, as were those with delay time (δt) errors of greater than 10%. The average delay time for the dataset is 35 ms, but these range from 2 ms to a maximum of 80 ms. Figure 6 shows that the fast-shear wave polarisations cluster around the direction perpendicular to the flow of the ice stream, whilst the initial source polarisations cluster around the direction of ice flow. It should be noted that a source polarisation that is exactly perpendicular to the fast shear-wave polarisation would result in a 'null' measurement. The more northerly event-station pairs gave generally better results due to the higher SNR at the more northerly stations.

Interpretation and discussion

Figure 7 shows the splitting results plotted in map view at the surface projection of the mid-point between the source and receiver. The diagram shows that the dominant fast shear wave polarisation (ϕ) is oriented perpendicular to the ice stream flow direction. It also shows the variability in the magnitude of the splitting (δt) but does not take into account variations in ray path directions. A better representation of the variation in splitting with ray azimuth and inclination is shown on an upper hemisphere projection of the results (Figure 8a). To aid interpretation of the results, and as the station array is located within the region of convergent flow on the ice stream, we consider each result as a sample of the same flow regime, but along varying ray directions.

We can rule out a simple VTI model of ice anisotropy, as there is significant splitting in the vertical directions and there is clearly significant variation in the magnitude of the splitting with ray azimuth (compare Figures 1 and 8a). This means that a cluster or solid-cone model alone does not fit the data. Based on the predictions of Azuma (1994) this is perhaps not surprising. In order to understand these variations in delay times and fast polarization directions between stations, we employ the shear wave splitting inversion technique proposed by Verdon et al. (2009). We assume a physical model for the anisotropy that is based on a single set of vertically aligned cracks superimposed on an intrinsically VTI medium, which yields an effectively orthorhombic medium. We then seek to find the model parameters that best fit our observations. This method finds the fracture parameters (strike and density) that best fit the observations. For more detail, the reader is referred to Verdon et al. (2009) and Wuestefeld et al. (2011).

A girdle model of ice anisotropy, where the Ih-crystal c-axes lie in a vertical plane normal to the flow direction is not inconsistent with the observations. This is in agreement with the predictions of Azuma (1994), as the microseismic survey is located close to the grounding line and therefore the ice stream outlet, meaning that the flow regime is likely convergent. Figure 8b shows the best fitting girdle model, assuming a hexagonal symmetry with the symmetry axis (a-axes clustering) oriented horizontally in the flow direction. It predicts the a-axis to be oriented at 162 ^{o} +/- 5^{o} (the ice stream flow direction is 165 degs N).

Finally, we consider a model where the anisotropy is due to vertically aligned cracks or melt films (hereafter simply referred to as cracks, as one cannot distinguish between these mechanisms without more detailed analysis of the data). As described above, we invert the data for a model with a background VTI symmetry that it superimposed with an HTI symmetry. The best fitting model is shown in Figure 8c. The VTI component could be attributed to a solid-cone or cluster model and the HTI component is due to orientated cracks. The VTI component is not well constrained as there is a lack of near-horizontal raypaths. In contrast, the HTI component is well constrained and is best fit by a crack set with a strike of 55^{o} +/- 10 ^{o} (or 145 ^{o}) (i.e., which is roughly 15^{o} from the

normal to flow direction) and a fracture density of 0.046 (crack-density = $N r^3 / V$, where *'N'* is the number of cracks in a volume, *'V'*, and *'r'* is the average crack radius, assuming penny-shaped cracks (Hudson, 1981)). For the best fitting model, the maximum contribution to the anisotropy from aligned cracks is roughly 4%.

In attempt to assess which models best fit the data we calculate the residual misfit for both the shear-wave polarisations and the splitting magnitudes. We compute modelled shear wave splitting parameters for each azimuth and inclination present in the observed dataset. We compute the rms misfit for polarisation direction and magnitude separately, and normalise each by their minimum values before summing them to give an overall misfit. The different normalisation factors for each model makes a direct comparison of the combined misfit difficult, however comparisons can be made for the individual misfit values. The VTI (cluster) model gives the worst fit to the data. Based on polarisations (ϕ), the HTI models (either the girdle fabric or crack-induced anisotropy) fit the data better than the VTI or VTI+HTI models. In contrast, based on misfit in splitting magnitudes (δt), the VTI+HTI mechanism is the best fitting models. Without further data it is difficult to discriminate any further between models. Ideally, one would combine both misfit calculations (i.e., both ϕ and δt), but the relative weighting for each is a bit arbitrary.

Without more data it is difficult to discriminate between the girdle model and the crack model as an explanation for the HTI component of the anisotropy. It is conceivable that both mechanisms are at play, but perhaps with different intensities at different depths or with varying distance from the flanks of the ice stream. The crack hypothesis would require a dominant alignment in the direction perpendicular to the direction of ice stream flow.

There are a number of steps that could be taken to improve certainty in the best fitting model of ice anisotropy. Analysis of P-wave anisotropy would be complimentary – perhaps using controlled source seismic refraction and reflection experiments. Azimuthal variations in P-wave velocities (e.g., Bentley, 1971) and/or amplitudes (Hall and Kendall, 2003) will be indicative of non-VTI models. Alternatively, non-hyperbolic moveout in seismic reflections is indicative of VTI anisotropy (e.g., van der Baan and Kendall, 2002). Finally, the

364 combined analysis of body wave and surface wave data helps constrain the
365 spatial patterns and mechanisms of anisotropy (e.g., Brisbourne, et al., 1999;
366 Snyder and Bruneton, 2007).
367 Ideally a denser array of sensors is needed to look at lateral variations
368 across the ice stream. This would allow better testing of the Azuma (1994)
369 model. It would also be nice to have some control on depth variability in the
370 anisotropy. Unfortunately, the icequakes at Rutford seem to be confined to the
371 ice-bed. Another approach is to use borehole data. Three-component borehole
372 sensors can be deployed in an array to record icequakes, as is commonly used in
373 monitoring hydraulic stimulation of petroleum reservoirs (e.g., Wuestefeld et al.,
374 2011). This avoids problems with the more attenuative near surface and
375 removes issues of the shear wave window (i.e., there is no free-surface effect).
376 Therefore one can record raypaths closer to horizontal and better discriminate
377 between models. Finally, borehole sensors and a shear wave surface source
378 would also help constrain depth variations in ice anisotropy.
379 Ice streams sometimes change in speed and orientation. Identifying these
380 variations may provide important first indications of possible ice stream
381 disintegration and acceleration, as has recently occurred on the Larsen B ice
382 shelf. Post-break up, Scambos et al. (2004) identified changes in glacier velocity
383 using GPS. However, any evidence of temporal variations in shear-wave splitting
384 could be used to track such changes closer to real time and more importantly,
385 determine how quickly rheology responds to such change. Stress changes
386 associated with hydraulic stimulation have been documented in both petroleum
387 (Wuestefeld et al., 2011) and volcanic settings (Johnson et al., 2010) using
388 observations of shear wave splitting.
389
390 **Conclusions**
391 Shear wave splitting has been measured in 41 icequakes from the base of
392 the Rutford ice stream recorded by an array of 5 seismometers deployed at the
393 surface near the grounding line. The events are located using S-P travel time
394 residuals and are consistent with a stick-slip mechanism. The events cluster in
395 regions, suggesting the locations of points where the friction between the ice and
396 bedrock is highest.

We observe large variations in the magnitude of the shear-wave splitting (2 ms – 80 ms) and the polarisation of the fast shear wave is dominantly orthogonal to the flow of the ice stream. The average magnitude of the shear-wave anisotropy for the entire thickness of the sheet is a maximum of 6% (the anisotropy may be higher if confined to more localised regions).

We consider three causes of the anisotropy. The first is a solid-cone or cluster model, where the c-axes orient in a subvertical cone. This produces a VTI symmetry. Previous results have shown that the angle the cone makes with the vertical should decrease as the confining pressure increases. This model predicts very little shear-wave splitting for vertical wave propagation, which is inconsistent with the observations. We therefore conclude that this model alone cannot explain the results. We next consider the girdle model where the c-axes align in a vertical plane perpendicular to the ice stream flow, with a concentration of a-axes parallel to the flow direction. This produces an HTI symmetry. This model explains the observations for sub-vertical raypaths. We finally consider a model that is a combination of a VTI and HTI symmetry (i.e., an orthorhombic symmetry). With the data available it is difficult to constrain the VTI component of the anisotropy, and, as such, both HTI and orthorhombic models are viable.

There are two possible explanations for a model with both a VTI and HTI component. The first is a cluster (solid-cone) model with a set of vertically oriented cracks aligned roughly perpendicular to the flow direction. Such cracks may be in response to undulations in bedrock topography, or be due to much smaller melt films that are aligned by the stress field. Alternatively, the composite model may be due to the accrued anisotropy through a cluster model near the ice bed and a girdle model in the upper parts of the ice stream. Such a model is consistent with the predictions of Azuma (1994). Bentley (1972) observed vertical variations in the style and magnitude of ice anisotropy near the Byrd station drill hole and further support comes from petrofabric analysis of core data (Obbard and Baker, 2007).

Future icequake monitoring experiments with both surface and borehole sensors would provide a detailed picture of vertical variations in ice anisotropy, which would be invaluable for calibrating ice flow models that include

anisotropic rheologies. We have presented the first documented observation of shear wave splitting in icequakes, and the initial results suggest that this is a fruitful means of better quantifying in-situ ice anisotropy.

Acknowledgements

We thank the editors Matt King and Bernd Kulessa for handling the manuscript and acknowledge the helpful comments of two reviewers, which improved the manuscript. SEIS-UK is acknowledged for the loan of equipment (NERC Geophysical Equipment Facility, Loan Number 852) and we thank BAS Operations and Chris Griffiths for field support. This study is part of the British Antarctic Survey Polar Science for Planet Earth Programme and was funded by The Natural Environment Research Council (NE/B502287/1). Rachel Obbard (from Thayer College) is acknowledged for her EBSD results and advice on ice crystal fabrics.

References

Acharya, H. K. 1972. Surface-wave dispersion in Byrd Land, Antarctica, *Bull. Seism. Soc. Am., 62*, 955-959.

Alley, R. B., 1988. Fabrics in polar ice sheets: Development and prediction, Science, 240, 493-495, DOI:10.1126/science.240.4851.493.

Anandakrishnan, S. and C.R. Bentley. 1993. Micro-earthquakes beneath Ice Streams B and C, West Antarctica: observations and implications, *J. Glaciol., 39(133),* 455–462.

Anandakrishnan, S. and R.B. Alley. 1994. Ice Stream C, Antarctica, sticky spots detected by microearthquake monitoring, *Ann. Glaciol., 20*, 183–186.

Anandakrishnan, S., J. J. Fitzpatrick, R. B. Alley, A. J. Gow and D. A. Meese. 1994. Shear-wave detection of asymmetric *c*-axis fabrics in the GISP2 ice core, Greenland, *J. Glaciology, 40*, 491-496.

Azuma, N. 1994. A flow law for anisotropic ice and its application to ice sheets. *Earth and Planetary Science Letters, 128*, 601-614.

Backus, G. E. 1962. Long-wave elastic anisotropy produced by horizontal layering, *J. Geophys. Res., 67*, 4427–4440.

Bentley, C. R. 1964. The structure of Antarctica and its ice cover, in *Research in Geophysics*, *vol. 2, Solid Earth and Interface Phenomena*, 335-389.

Bentley, C. R. 1971. Seismic anisotropy in the West Antarctic ice sheet, in *Snow and Ice Studies II, Antarctic Re. Ser., 16*, edited by A. P. Crary, 131-178.

Bentley, C. R. 1972. Seismic-wave velocities in anisotropic ice: a comparison of measured and calculated values in and around the Deep Drill Hole at Byrd Station, Antarctica, *J. Geophys. Res*., *77*, 4406-4420.

Bentley, C. R. 1975. Advances in geophysical exploration of ice sheets and glaciers, *J. Glaciology, 15*, 113-135.

Blackman, D. K., H-R. Wenk and J-M. Kendall. 2002. Seismic anisotropy of the upper mantle: 1. Factors that affect mineral texture and effective elastic properties, *Geochem., Geophys. Geosystems, 3*, No.9, 8601, doi:10.1029/2001GC000248.

Booth, D.C. and Crampin, S. 1985. Shear-wave polarizations on a curved wavefront at an isotropic free surface, *Geophys. J. Roy. Astro. Soc., 83*, 31-45.

Budd, W. F. and T. H. Jacka. 1989. A review of ice rheology for ice sheet modelling, *Cold Regions Science and Technology, 16*, 107-144.

Brisbourne, A., G. W. Stuart and J-M. Kendall. 1999. Anisotropic structure of the Hikurangi subduction zone, New Zealand – Integrated interpretation of surface-wave and body-wave observations, *Geophys. J. Int., 137*, 214-230.

Brisbourne, A. 2012. How to store and share geophysical data. Astronomy & Geophysics, 53: 4.19-4.20. doi: 10.1111/j.1468-4004.2012.53419.x

Castelnau, O., P. Duval, R. Lebensohn and G.R. Canova. 1996. Viscoplastic modeling of texture development in polycrystalline ice with a self-consistent approach: comparison with bound estimates, *J. Geophys. Res., 101(B6),* 13,851–13,868.

Duval, P., M.F. Ashby and I. Anderman. 1983. Rate-controlling processes in the creep of polycrystalline ice, *J. Phys. Chem., 87(21)*, 4066–4074.

Gusmeroli, A., E. C. Pettit, J. H. Kennedy, and C. Ritz. 2012. The crystal fabric of ice from full-waveform borehole sonic logging, *J. Geophys. Res.*, *117*, F03021, doi:10.1029/2012JF002343.

Hall, S. A. and J-M. Kendall. 2003. Fracture characterisation at Valhall: Application of P-wave AVOA analysis to a 3D ocean-bottom data set, *Geophysics, 68*, 1150-1160.

Holtzman, B. K. and J-M. Kendall,. 2010. Organized Melt, Seismic Anisotropy and Plate Boundary Lubrication, *Geochem. Geophys. Geosyst*, *11*, Q0AB06, 29pp, doi:10.1029/2010GC003296.

Horgan, H. J., S. Anandakrishnan, R. B. Alley, P. G. Burkett and L. E. Peters. 2011. Englacial seismic reflectivity: imaging crystal-orientation fabric in West Antarctica, *J. Glaciology, 57*, 639-650.

Hudson, J. A. 1981. Wave speeds and attenuation of elastic waves in material containing cracks, *Geophys. J. Roy. Astro. Soc.*, *64*, 133-150.

Johnson, J. H., S. Prejean, M. K. Savage, and J. Townend. 2010. Anisotropy, repeating earthquakes, and seismicity associated with the 2008 eruption of Okmok volcano, Alaska, *J. Geophys. Res., 115*, B00B04, doi:10.1029/2009JB006991.

Kendall, J-M., Q. J. Fisher, S. Covey-Crump, J. Maddock, A. Carter, S. A. Hall, J. Wookey, S. L. A. Valcke, M. Casey, G. Lloyd and W. Ben Ismail. 2007. Seismic anisotropy as an indicator of reservoir quality in siliciclastic rocks, *Structurally Complex Reservoirs*, eds. S. Jolley, D. Barr, J. Walsh and R. J. Knipe, Geol. Soc. London – Spec. Pub., *292*, 123-136.

King, E. C. 2009. Flow dynamics of the Rutford Ice Stream ice-drainage basin, West Antarctica, from radar stratigraphy. *Annals of Glaciology*, 50 (51). 42-48.

Klein, F. 2000. HYPOINVERSE-2000, http://geopubs.wr.usgs.gov/open-file/of02-171,

Mader, H. M. 1992. Observations of the water vein system in polycrystalline ice, *J. Glaciology, 38*, 333-347.

Martin, C., G. H. Gudmundsson, H. Pritchard and O. Gagliardini. 2009. On the effects of anisotropic rheology on ice flow, internal structure, and the age-depth relationship at ice divides. *J. Geophys. Res., 114,* doi:10.1029/2008JF001204.

Morgan, V. I., T. H. Jacka, G. J. Akerman and A. L. Clarke. 1982. Outlet glacier and mass-budget studies in Enderby, Kemp, and Mac. Robertson lands, Antarctica, *Ann. Glaciol.*, *3*, 204-210.

Obbard, R. and I. Baker. 2007. The microstructure of meteoric ice from Vostok, Antarctica, *Journal of Glaciology, 53*, 41-62.

Pritchard, H. D., Brisbourne, A. M., King, E. C., Gudmundsson, G. H. and Smith, A. M. 2011. Scientific Report: Gauging Rutford Ice Stream Transients (GRIST). Natural

524 Environment Reseach Council (NERC) Report.
525 Roethlisberger, H. 1972. Seismic exploration in cold regions. *Cold Regions Science and*
526 *957 Engineering Monograph II-A 2a*. Hannover, N.H: Cold Reg. Res. and Eng. Lab.
527 Robinson, E. S. 1968. Seismic wave propagation on a heterogeneous polar ice sheet, *J.*
528 *Geophys. Res.* 73, 739-753.
529 Scambos, T.A.; Bohlander, J.A.; Shuman, C.A.; Skvarca, P. 2004. Glacier acceleration and
530 thinning after ice shelf collapse in the Larsen B embayment, Antarctica *Geophys.*
531 *Res. Lett. 31*: L18402(1-4)
532 Smith, A. M. 1997a. Basal conditions on Rutford Ice Stream, West Antarctica, from
533 seismic observations, *J. Geophys. Res.* 102, 543-552.
534 Smith, A. M. 1997b. Variations in basal conditions on Rutford Ice Stream, West
535 Antarctica, *Journal of Glaciology,* 43, 245-255.
536 Smith, A. M. 2006. Microearthquakes and subglacial conditions, *Geophysical Research*
537 *Letters*, 33, L24501.
538 Snyder, D. B. and M. Bruneton. 2007. Seismic anisotropy of the Slave craton, NW Canada,
539 from joint interpretation of SKS and Rayleigh waves, *Geophys. J. Int.*, *169*, 170-188.
540 Teanby, N., M. Van der Baan and J-M. Kendall, Automation of shear-wave splitting
541 measurements using cluster analysis, *Bull. Seis. Soc. Am., 94*, 453-463, 2004.
542 Thomsen, L. 1999. Converted-wave reflection seismology over inhomogeneous,
543 anisotropic media, *Geophysics, 64*, 678-690.
544 Van der Baan M. and J-M. Kendall. 2002. Estimating anisotropy parameters and
545 traveltimes in the tau-p domain, *Geophysics, 67*, 1076-1086.
546 Verdon, J.P., J-M. Kendall and A. Wustefeld. 2009. Imaging fractures and sedimentary
547 fabrics using shear wave splitting measurements made on passive seismic data,
548 *Geophys. J. Int., 179*, 1245-1254, 10.1111/j.1365-246X.2009.04347.x.
549 Walker, A.M., and Wookey, J. 2012. MSAT—A new toolkit for the analysis of elastic and
550 seismic anisotropy. *Computers and Geosciences. 49*, 81-90.
551 http://dx.doi.org/10.1016/j.cageo.2012.05.031.
552 Walter, F., N. Deichmann and M. Funk. 2008. Basal icequakes during changing subglacial
553 water pressures beneath Gornergletscher, Switzerland, *J. Glaciology, 54*, 511-521.
554 Wilson, C. 2000.
555 http://virtualexplorer.com.au/special/meansvolume/contribs/wilson/Contents.h
556 tml
557 Wilson, C.J.L. and Y. Zhang. 1994. Comparison between experiment and computer
558 modeling of plane-strain simple-shear ice deformation, *J Glaciology, 40*, 46-53.
559 Wuestefeld, A., O. Al-Harrasi, J. P. Verdon, J. Wookey and J-M. Kendall. 2010. A strategy
560 for automated analysis of passive microseismic data to image seismic anisotropy
561 and fracture characteristics, *Geophys. Prosp*, 58, 755-773, 2010. doi:
562 10.1111/j.1365-2478.2010.00891.x.
563 Wuestefeld. A., J. P. Verdon, J-M. Kendall, J. Rutledge, H. Clarke and J. Wookey. 2011.
564 Inferring rock fracture evolution during reservoir stimulation from seismic
565 anisotropy, *Geophysics, 76*, WC157-WC166.
566

Figures

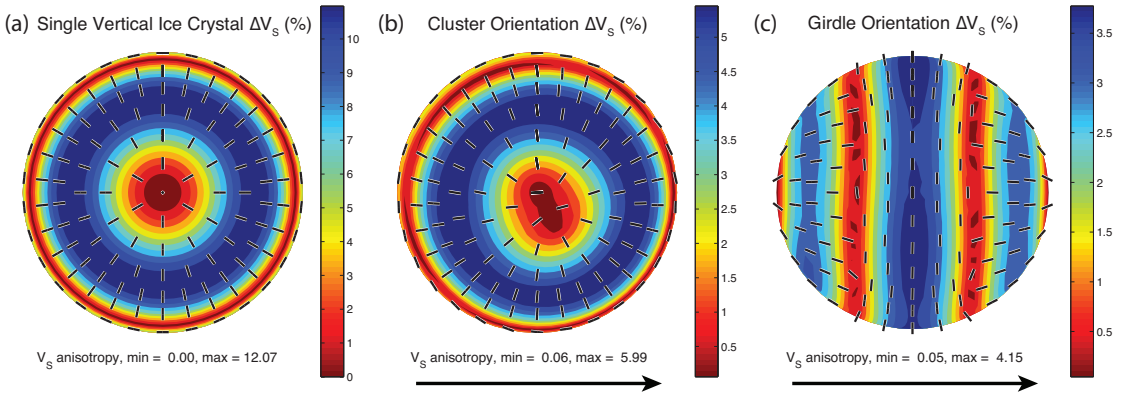

Figure 1. Upper-hemisphere projections of the predicted shear-wave splitting due to the alignment of Ih-crystal ice (produced using the MSAT package of Walker and Wookey (2012)). Tick marks show the polarization of the fast shear-wave. Red colours show regions of minimum shear-wave splitting, blue colours show regions of maximum splitting. The maximum and minimum values are also displayed below each projection. The black arrows indicate ice flow direction. (a) Single crystal of Ih-hexagonal ice. (b) The 'cluster' or 'solid-cone' model, which is due to the alignment of c-axes in a cone around the vertical direction. (c) The 'girdle' model, where the a-axes are aligned in the horizontal direction parallel to the flow direction and the c-axes are aligned in a vertical plane perpendicular to this.

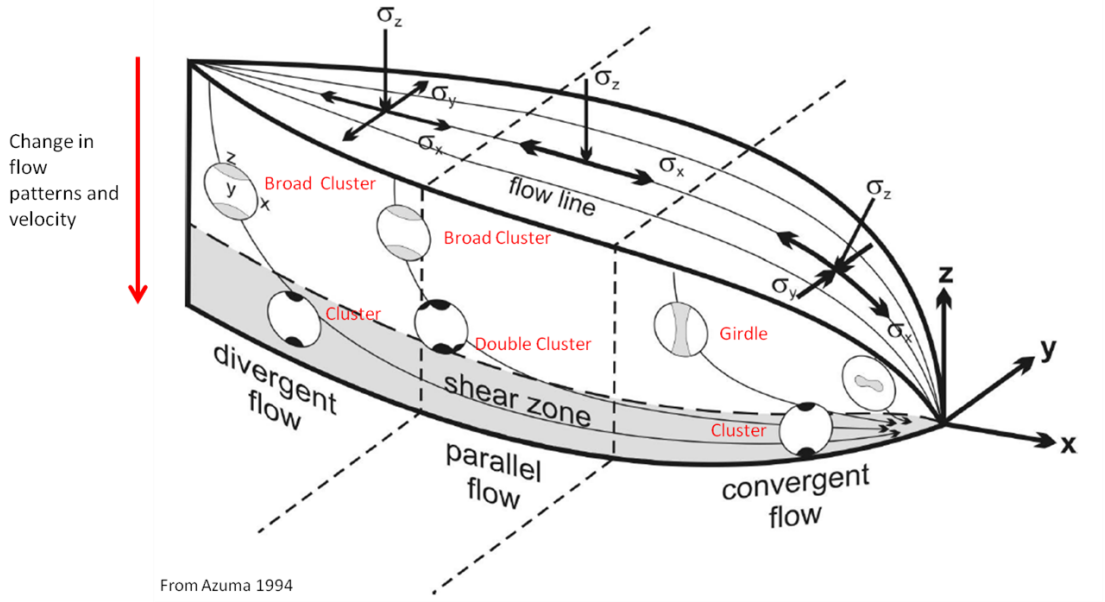

Figure 2. Predictions of ice-crystal fabric in an ice-stream. Modified from Azuma (1994). Three flow regimes are indicated: divergent, parallel, and convergent flow; and the corresponding stress (σ) regimes are indicated above. A basal shear zone consistently shows a cluster or solid-cone distribution in c-axes, although a double cluster is predicted in the region of parallel flow. A transition from a cluster model to a girdle model as the flow becomes convergent.

589

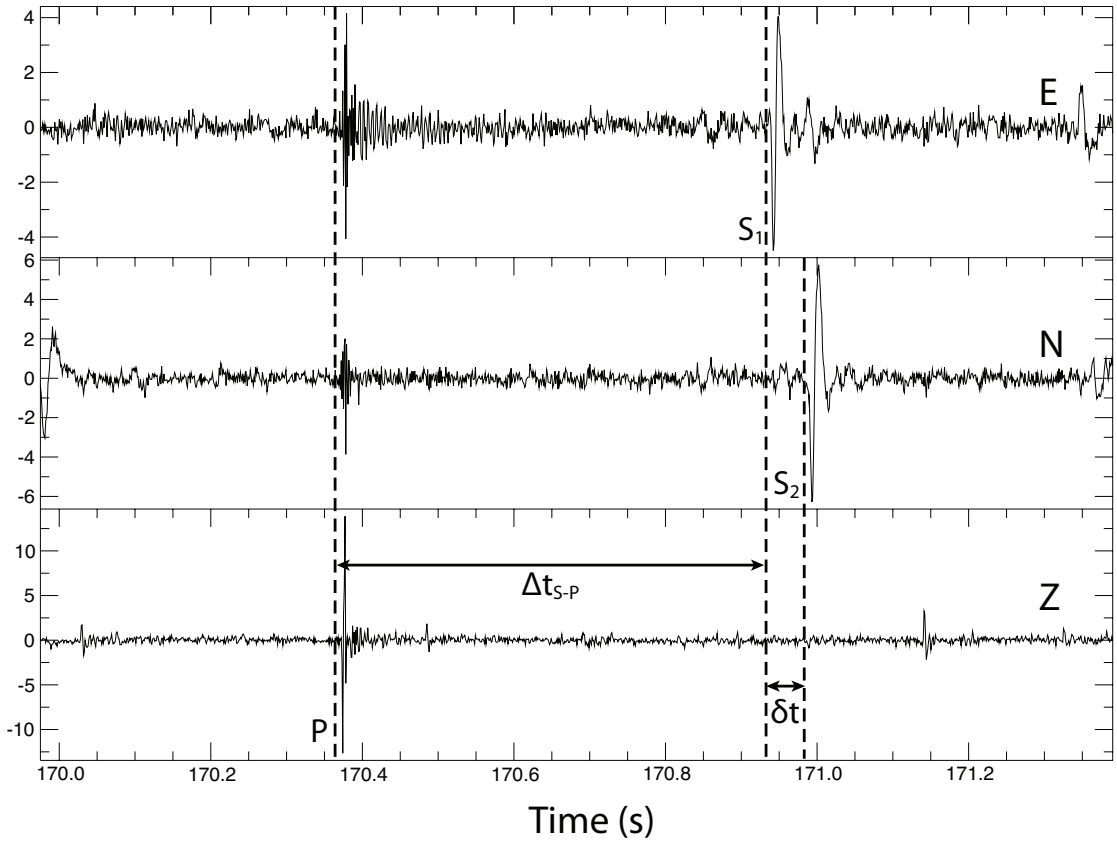

590

591

592 **Figure 3.** An example of a typical icequake recorded at station 1. The P-wave (P),
593 fast shear-wave (S1) and slow shear-wave (S2) are marked. The S-P travel time
594 used to locate the event is marked Δt_{S-P} and the delay time between the fast and
595 slow shear wave is marked δt.
596

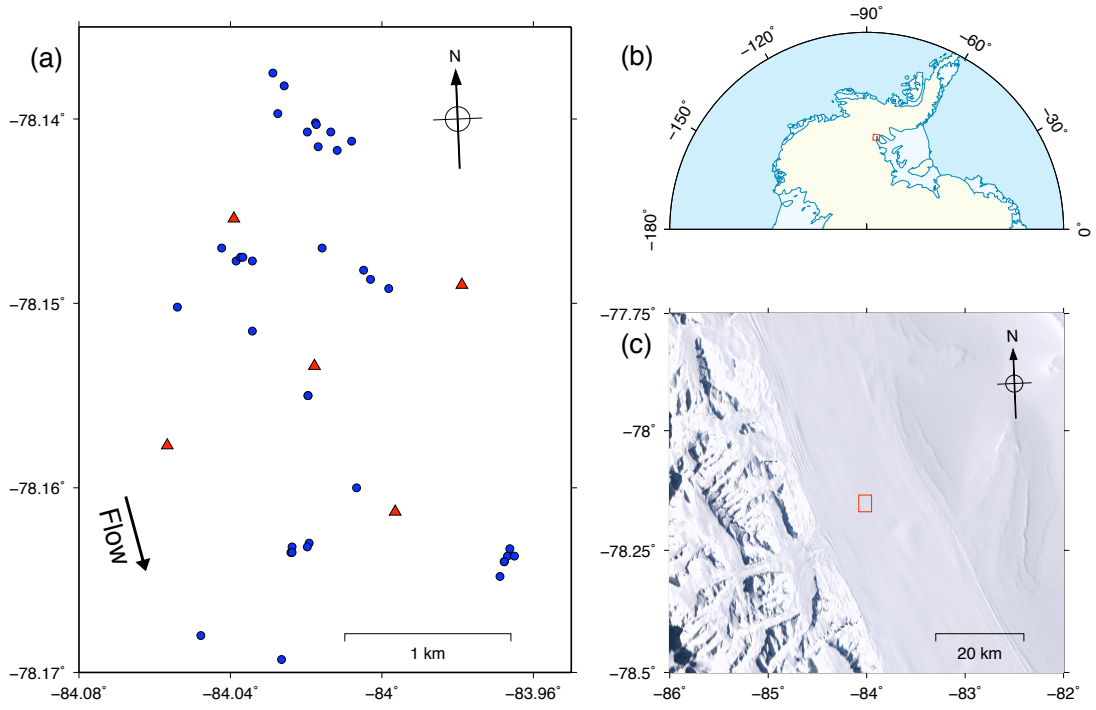

Figure 4. Location of seismic stations, icequake epicentres and the location of the microseismic experiment. (a) epicentres are shown in blue and stations in red; the arrow indicates the flow direction of the ice stream. (b) red square indicates location of experiment. (c) red square indicates location of experiment on map showing the surface elevation of the Rutford ice stream (natural color Landsat image). The flow direction of the ice stream is ~165°.

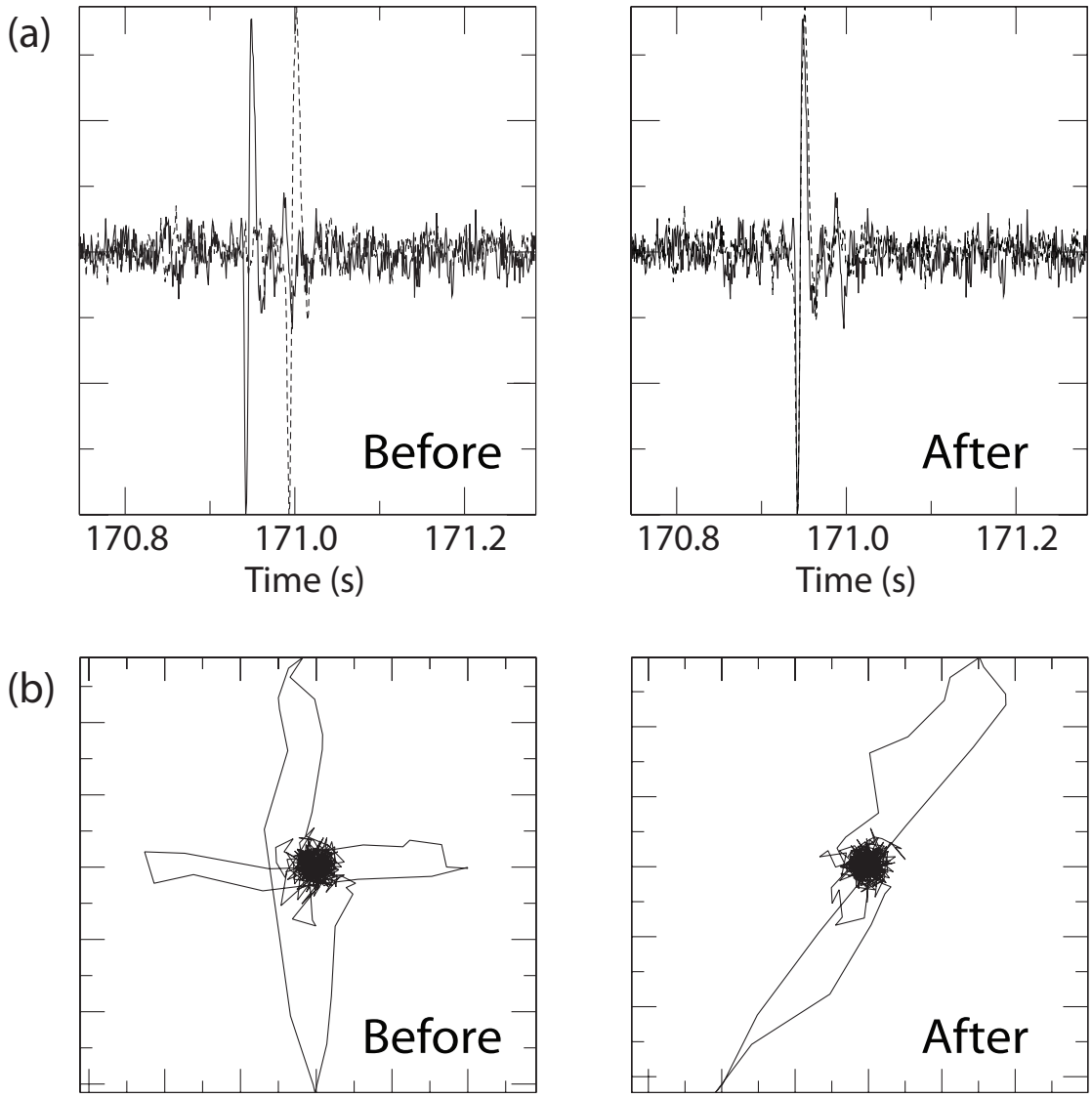

606

607 **Figure 5**. An example of a shear wave splitting measurement made on the
608 icequake record shown in Figure 3. (a) shows the fast and slow shear-waves
609 before and after correcting for the shear wave splitting. (b) shows the shear-
610 wave particle motion before and after determining the shear-wave splitting
611 parameters that best linearise the particle motion.
612

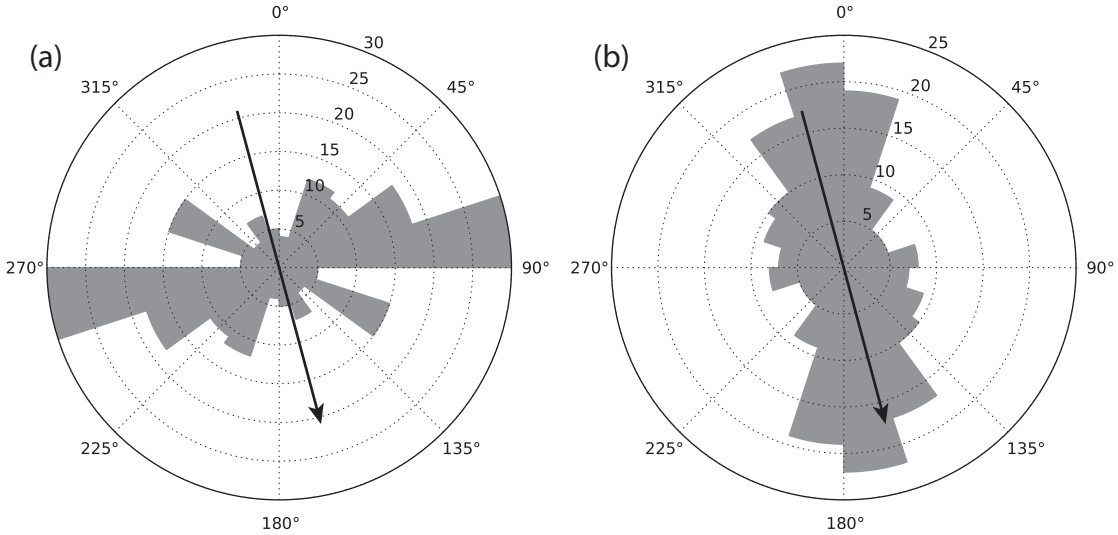

Figure 6. Rose diagrams for (a) fast shear polarizations and (b) initial source polarizations for the entire set of shear wave splitting measurements. The heavy black arrow indicates the ice flow direction.

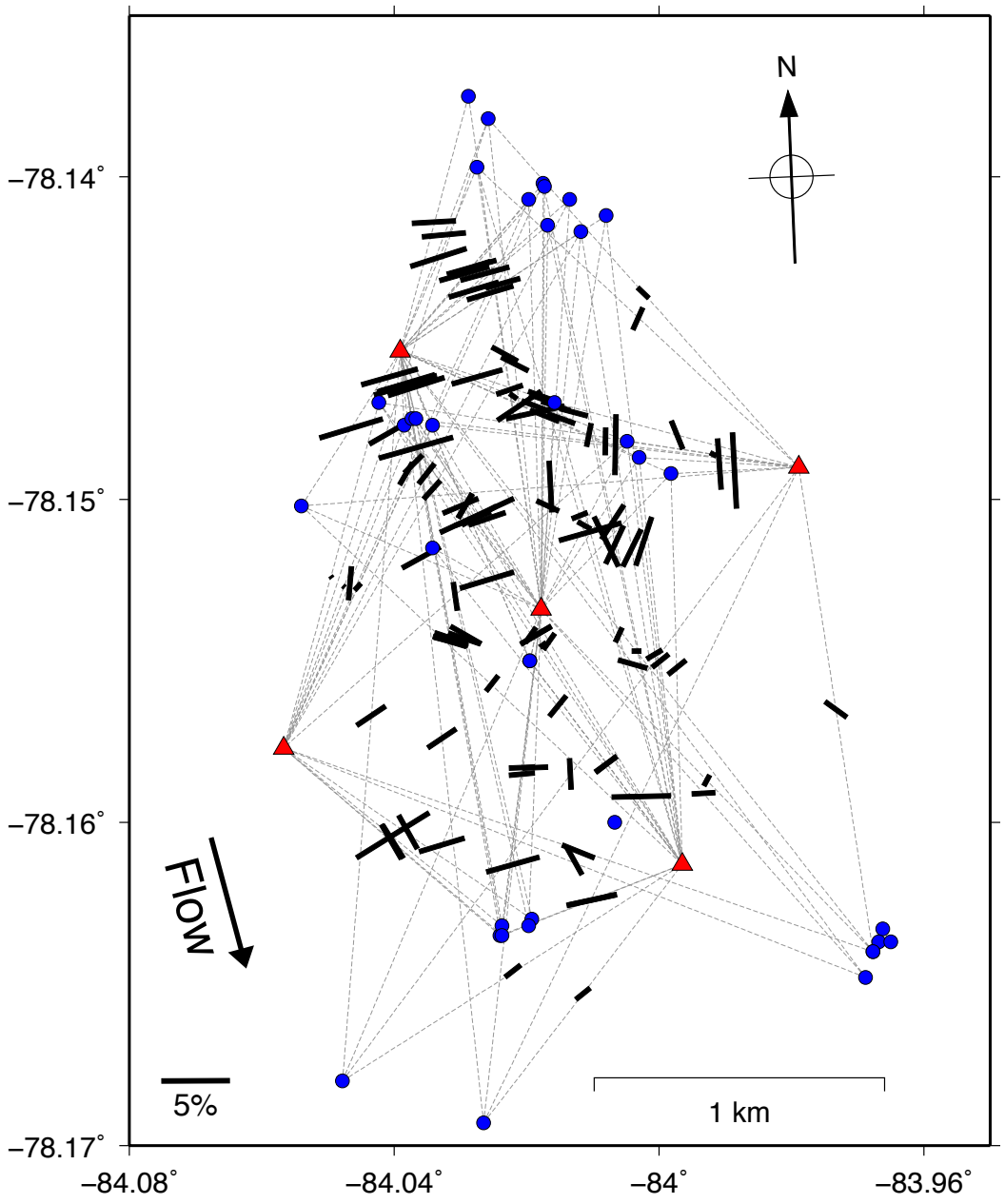

618

619 **Figure 7**. A map view of the shear wave splitting results. The events (blue
620 circles) and stations (red triangles) are marked and the splitting measurement is
621 plotted at the midpoint of the raypath (dashed line). The tick length is
622 proportional to the magnitude of the splitting and the tick orientation shows the
623 polarisation of the fast shear wave. The flow direction of the ice stream is 165°.

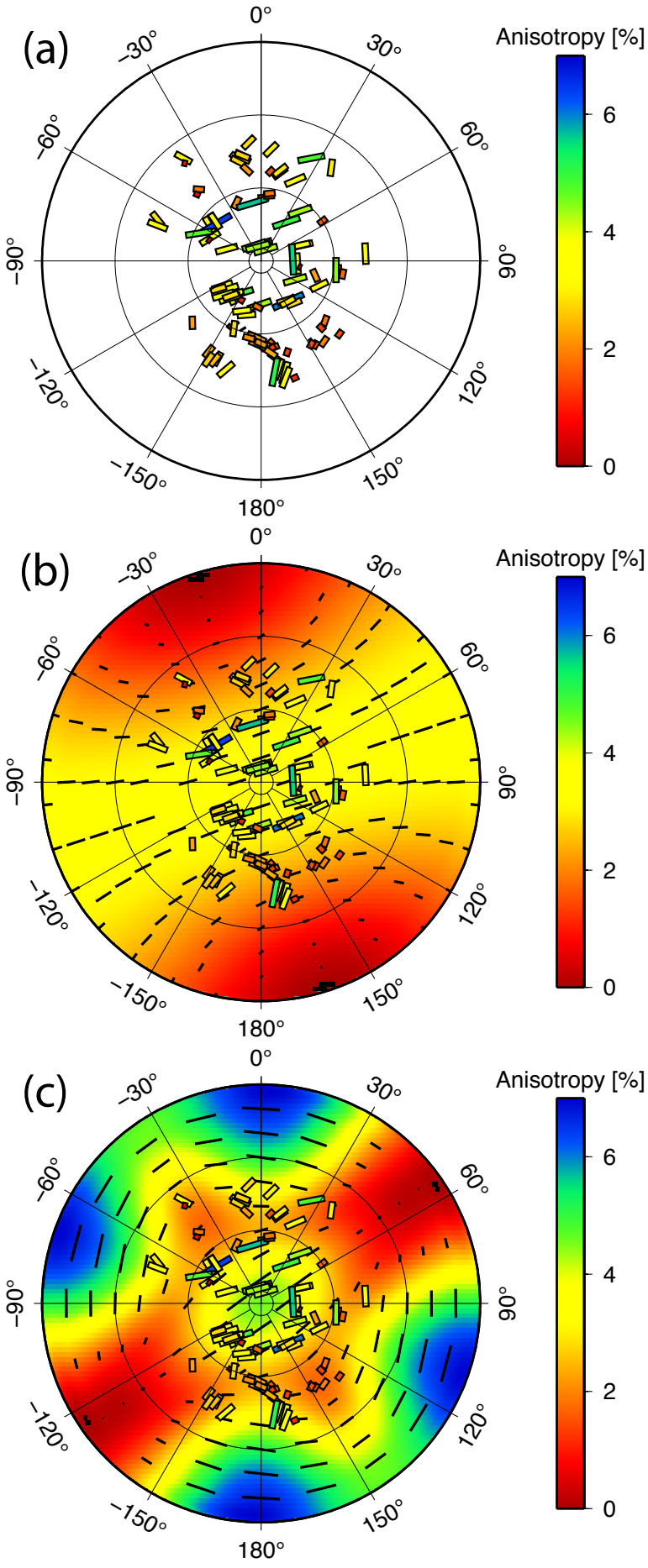

624

Figure 8. (a) The shear wave splitting results plotted on an upper hemisphere projection. Vertical raypaths plot at the centre and horizontally propagating rays would plot at the edge. The tick colour and length is proportional to the magnitude of the splitting and its orientation shows the polarisation of the fast shear wave. (b) As in (a), also showing the HTI model that best fits the shear wave splitting measurements. This shows the orientation and magnitude of splitting for the girdle model that best explains the data. Black ticks show the orientation of the fast shear wave polarisation and their length is proportional to the splitting. Colour scale indicates the magnitude of the anisotropy. (c) As in (a), but also showing the orthorhombic model that best fits the shear wave splitting measurements. The data are inverted for a model with vertically aligned cracks superimposed on a model with VTI symmetry. Black ticks show the orientation of the fast shear wave polarisation predicted by the model and their length is proportional to the splitting. Ticks with a white outline are the fast shear wave polarisations for the observations. Colour scale indicates the magnitude of the anisotropy.